Dear author,

Please note that changes made in the online proofing system will be added to the article before publication but are not reflected in this PDF.

We also ask that this file not be used for submitting corrections.

International Journal of Solids and Structures xxx (xxxx) xxx

Contents lists available at ScienceDirect

International Journal of Solids and Structures

journal homepage: www.elsevier.com/locate/ijsolstr

Buckling of a Timoshenko beam bonded to an elastic half-plane: Effects of sharp and smooth beam edges

Q2 F.O. Falope [a,c,*], L. Lanzoni [a,c,d], E. Radi [b,c]

[a] University of Modena and Reggio Emilia, Dipartimento di Ingegneria “Enzo Ferrari”, DIEF, Via P. Vivarelli 10, Modena, 41125, Italy
[b] University of Modena and Reggio Emilia, Dipartimento di Scienze e Metodi dell'Ingegneria, DISMI, Via G. Amendola 2, Reggio Emilia, 42122, Italy
[c] CRICT - Centro Interdipartimentale di Ricerca e per i Servizi nel Settore delle Costruzioni, via P. Vivarelli 10, Modena, 41125, Italy
[d] Centro Interdipartimentale “En&Tech”, via G. Amendola, 2, Reggio Emilia, 42122, Italy

ARTICLE INFO

Article history:
Received 14 May 2019
Revised 25 July 2019
Accepted 27 August 2019
Available online xxx

Keywords:
Buckling load
Elastic half-plane
Edge effects
Timoshenko beam
Frictionless contact
Chebyshev polynomials

ABSTRACT

The problem of a compressed Timoshenko beam of finite length in frictionless and bilateral contact with an elastic half-plane is investigated here. A Chebyshev series solution is found and, for some limiting cases, an analytic form solution is provided. The problem formulation leads to an integro-differential equation which can be transformed into an algebraic system by expanding the rotation of the beam cross sections in series of Chebyshev polynomials. An eigenvalue problem is then obtained, whose solution provides the buckling loads of the beam and, in turn, the corresponding buckling mode shapes. Beams with sharp or smooth edges are considered in detail, founding relevant differences. In particular, it is shown that beams with smooth edges cannot exhibit a rigid-body buckling mode. A limit value of the soil compliance is found for beam with sharp edges, below which an analytic buckling load formula is provided without loss of reliability. Finally, in agreement with the Galin solution for the rigid flat punch on a half-plane, a simple relation between the half-plane elastic modulus and the Winkler soil constant is found. Thus, a straightforward formula predicting the buckling loads of stiff beams resting on compliant substrates is proposed.

1. Introduction

The knowledge of the critical load of elastic bars, beams, plates, shell panels and layered systems bonded to a deformable support is a key task for many engineering problems with specific reference to foundation beams, bridge decks, end-bearing piles and thin-film based devices (MEMS and NEMS) or composite systems (Bazant and Cedolin, 2003; Foraboschi, 2009). The buckling problem is usually formulated as an eigenvalue problem, whose solution provides both the buckling loads and the corresponding mode shapes.

In general, the mechanical interaction between an elastic beam and the underlying substrate involves both shear and normal (peeling) stresses (Falope et al., 2018). However, in many practical applications the shear stress is usually small and thus it can be neglected according to the simplifying assumption of frictionless contact (Reynolds, 1886). Moreover, the weight forces hinder the lifting of the beam from the substrate, thus making reasonable the assumption of bilateral contact for a wide class of practical cases.

The simplest model adopted in order to simulate an elastic support is the Winkler soil (WS). In this case, the support is represented by a series of discrete infinitesimal and mutually independent elastic springs. These springs provide to the beam axis a distributed transverse reactive pressure proportional to the beam deflection through the Winkler constant k. The soil stiffness is thus represented by a single substrate constant. As a consequence of its simplicity, many Authors extensively used such a scheme to investigate the buckling of beams on a deformable support (Timoshenko and Gere, 1961; Biot, 1957; Hetényi, 1971). Since its proposal, the Winkler model was subjected to a strong criticism by Wieghardt (1922) and many others owing to the fact that it leads to a rough approximation of the displacement field. Therefore, a non-local generalization of the Winkler model was later introduced by Wieghardt, who assumed that the contact pressure depends locally both on the deflection and curvature of the beam through two distinct parameters. The buckling problem of a beam laying on a Wieghardt soil was investigated in Smith (1969), Ruta and Elishakoff (2006).

* Corresponding author at: University of Modena and Reggio Emilia, Dipartimento di Ingegneria “Enzo Ferrari”, DIEF, Via P. Vivarelli 10, 41125, Modena, Italy.
E-mail addresses: federicooyedeji.falope@unimore.it (F.O. Falope), luca.lanzoni@unimore.it (L. Lanzoni), enrico.radi@unimore.it (E. Radi).

https://doi.org/10.1016/j.ijsolstr.2019.08.034
0020-7683/© 2019 Published by Elsevier Ltd.

Accurate analyses of the interaction between a beam and an underlying substrate can be performed by simulating the substrate (larger enough than the supported element) as a 2D semi-infinite elastic medium. Such an approach has been pursued by Shield and Kim (1992) in order to study an Euler-Bernoulli (E-B) beam resting on an incompressible elastic half-plane subjected to a uniform remotely applied strain. These authors also accounted for a shear-type cohesive zone at the interface in the neighbouring of the beam ends. Later, Lanzoni and Radi (2016) extended the analysis by considering a shear deformable Timoshenko beam resting on an elastic and isotropic half-plane and loaded by transversal forces. In this case, a complex power stress singularity is found at the beam ends, which depends on the Poisson ratio of the half-plane. Moreover, in proximity of the inner section of a Timoshenko beam loaded by a concentrated transversal force the pressure distribution between the beam and the half-plane displays a logarithmic singularity and the shear stress is finite and discontinuous across the loaded section, whereas for the E-B beam model the pressure was found regular therein. Accurate numerical studies about the interfacial stresses between bars and beams and an elastic 2D half-plane can be found in Tezzon et al. (2016), recently extended to a 3D half-space (Baraldi and Tullini, 2018).

The effect of a compressive load acting on an E-B beam resting on an elastic half-plane has been investigated by Gallagher (1974) by using a Chebyshev series expansion for representing the beam deflection. This Author considered special boundary conditions (BCs) for the beam, which was indeed assumed simply supported at the edges, hinged. However, the model of a continuum medium cannot sustain the concentrated loads that the supports can provide.

By using a coupled FE-BIE formulation involving the half-plane Green function, Tullini et al. (2012, 2013) numerically solved the buckling problem of Timoshenko beam in contact with an elastic half-plane under various BCs. Except for the Gallagher work (Gallagher, 1974), concerning E-B beam model, the aforementioned investigations are based on numerical approaches and, to Authors knowledge, a comprehensive analytical study on the stability of a Timoshenko beam bonded to an elastic half-plane cannot be found in Literature.

In the present work, the 2D problem of a compressed Timoshenko beam of finite length in frictionless and bilateral contact with an elastic and isotropic half-plane is investigated. Based on the relation between the interfacial reactive pressure and the displacement field, according to the Green function for an elastic half-plane loaded at its free surface, the problem is found to be governed by an integro-differential equation. The governing equation is then reduced to an algebraic system by expanding the rotation of the beam cross sections in series of Chebyshev polynomials of the first kind. Two dimensionless parameters, denoting the bending and shear stiffness of the beam with respect to (w.r.t.) that of the half-plane, completely characterize the system. The beam is considered free at its edges, thus requiring the vanishing of both the bending moment and the beam shear force resultant therein. Two different kinds of beam edges are considered in detail, namely sharp and smooth edges, which affect the distribution of the peeling stress within the contact region. For convenience, the corresponding eigenvalue problem for even and odd modes is formulated separately and then solved for the buckling loads. The results, provided in terms of fast convergent series expansion, show that the edge shape has a strong influence on the buckling load. In particular, it is shown that a beam with smooth edges can not exhibit a rigid-body critical buckling mode, differently from a beam with sharp edges.

The paper is organized as follows: The problem formulation and the BCs are presented in Section 2. The solution is worked out in Section 3 for even and odd buckling modes separately, whereas the main results are reported and commented within Section 4. In particular, some reference cases have been analysed in Section 4.1. The convergence rate of the series solution varying the governing parameters has been also investigated therein. The buckling of a rigid beam resting on an elastic half-plane is discussed in Sections 4.2 and 4.3 and relevant differences are found between the two kinds of beam edges. Finally, conclusions are drawn in Section 5.

2. Problem formulation

2.1. Governing equations

Let us consider a Timoshenko beam of length $2a$ in frictionless and bilateral contact with an elastic half-plane. Two opposite compressive axial forces P act at the beam edges as sketched in Fig. 1.

The interfacial shear stress will be neglect in the following.[1]

The plane problem is formulated per unit depth. The beam is characterized by the Young and shear moduli E_b and G_b, the moment of inertia I_b and the shear area $A_b^* = A_b/\chi$, being A_b the beam cross section area and χ its shear factor. The contact domain between the beam and the half-plane coincides with the entire beam length $2a$. The elastic half-plane is characterized by the Young modulus $\bar{E}_h$, being $\bar{E}_h = E_h/(1-\nu_h^2)$ or $\bar{E}_h = E_h$ for plane strain or generalized plane stress, respectively, and ν_h is the Poisson ratio.

The reference system origin is placed at the middle-span of the beam with the x axis rightward directed along the contact region, as reported in Fig. 1. At the interface the beam is subjected to the peeling stress $q(x)$ exchanged with the underlying substrate. It is worth noticing that the effect of the compressive axial forces P is equivalent to a temperature load (Falope et al., 2016) ΔT according to $P = E_b h[(1+\nu_h)\alpha_h - (1+\nu_b)\alpha_b]\Delta T$ or $P = E_b h[\alpha_h - \alpha_b]\Delta T$ for plane strain or plane stress, respectively, where α_i represents the coefficient of thermal expansion and subscripts "h" and "b" denote the half-plane and beam amount.

For the Timoshenko beam, the beam deflection $v(x)$ and its cross sections rotation $\varphi(x)$ are related by the following kinematic relation

$$\varphi(x) = -v'(x) + \gamma(x), \tag{1}$$

where $\gamma(x)$ is the shear strain and the apex denotes differentiation w.r.t. the spatial variable x. The constitutive relations connecting the bending moment $M(x)$ and shear stress resultant $T(x)$ with the curvature $\varphi'(x)$ and shear compliance $\gamma(x)$ read

$$M(x) = E_b I_b \varphi'(x), \quad T(x) = G_b A_b^* \gamma(x). \tag{2}$$

For convenience, the vertical stress resultant $V(x)$ will be introduced in the following. Under the assumption of small deformations, the balance conditions of an infinitesimal beam element of length dx (see Fig. 2) in the deformed configuration yield the following relations (Timoshenko and Gere, 1961):

$$V'(x) = -q(x), \quad T(x) = M'(x) = V(x) + Pv'(x). \tag{3}$$

By combining Eqs. (1)–(3), a third-order ODE in the rotation field is found:

$$E_b I_b \left(1 - \frac{P}{G_b A_b^*}\right)\varphi'''(x) + P\varphi'(x) + q(x) = 0. \tag{4}$$

[1] The shear stress arising at the interface can be accounted for by introducing an additional compatibility condition between the beam and the half-plane strains along the x direction (Lanzoni and Radi, 2016). This leads to a strongly non-linear integro-differential equation which can be solved only by numerical approaches. Since the condition of shear has been neglected, the contact pressure is directly applied to the beam axis.

Please cite this article as: F.O. Falope, L. Lanzoni and E. Radi, Buckling of a Timoshenko beam bonded to an elastic half-plane: Effects of sharp and smooth beam edges, International Journal of Solids and Structures, https://doi.org/10.1016/j.ijsolstr.2019.08.034

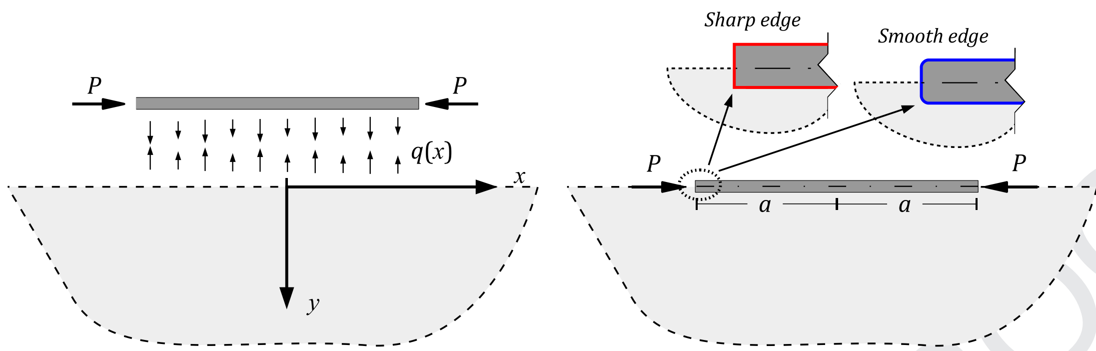

Fig. 1. Reference system.

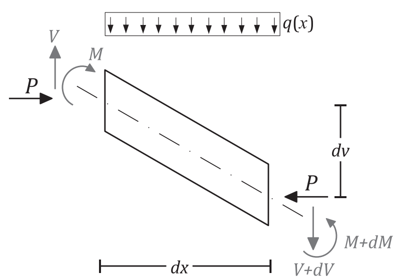

Fig. 2. Free-body diagram of an infinitesimal beam element in the deformed configuration.

The governing Eq. (4) highlights the coupling between the beam and half-plane through the interfacial normal stress $q(x)$ (peeling or pressure).

Two different kinds of beam edges are considered: *sharp edges* and *smooth edges*, which induce (square-root) singular or vanishing pressure at the edges, respectively, namely $q(\pm a) \to \infty$ or $q(\pm a) = 0$. As known from Muskhelishvili (2013), the peeling stress can be expressed as a function of the half-plane surface displacement according to the Cauchy integral

$$q(x) = \frac{\overline{E}_h}{2\pi}\frac{1}{\mathcal{K}(x/a)}\int_{-a}^{+a}\frac{\mathcal{K}(t/a)}{t-x}v'(t)\,dt, \tag{5}$$

where

$$\mathcal{K}(t) = \begin{cases}\sqrt{1-t^2}, & \text{for sharp beam edges,}\\ \dfrac{1}{\sqrt{1-t^2}}, & \text{for smooth beam edges,}\end{cases}$$

is here termed *edges function*.[2] By introducing the dimensionless spatial variable $\xi = x/a$, based on Eqs. (1) and (5), the governing Eq. (4) provides the following integro-differential equation for the rotation field $\varphi(\xi)$

$$(1-\tilde{P}\rho)\varphi'''(\xi) + \tilde{P}\varphi'(\xi) + \frac{\kappa}{2\pi}\frac{1}{\mathcal{K}(\xi)} \times \int_{-1}^{+1}\frac{\mathcal{K}(s)}{s-\xi}[\rho\varphi''(s) - \varphi(s)]\,ds = 0, \tag{6}$$

where $\tilde{P} = Pa^2/E_bI_b$ is the normalized axial load and

$$\kappa = \frac{\overline{E}_h a^3}{E_b I_b}, \quad \rho = \frac{E_b I_b}{a^2 G_b A_b^*}, \tag{7}$$

are two dimensionless parameters denoting the beam flexural compliance compared to the half-plane stiffness and the ratio between the beam bending stiffness and shear stiffness, respectively. In the following, κ and ρ will be called *stiffness parameter* and *shear parameter*, respectively.

The beam edges are assumed as free. Accordingly, the BCs require the bending moment M and vertical force V vanishing, namely, by using Eqs. (2) and (3)

$$\varphi' = 0, \quad (1-\tilde{P}\rho)\varphi'' + \tilde{P}\varphi = 0, \quad \text{for } \xi = \pm 1. \tag{8}$$

3. Problem solution

3.1. Solution strategy

The problem is approached by expanding the rotation field second derivative $\varphi''(\xi)$ in series of Chebyshev polynomials of the first kind $T_n(\xi)$. Once the integral pressure term (5) has been evaluated in closed form, the governing equation is transformed into an infinite series of Chebyshev polynomials with unknown coefficients C_n. Then, the Galerkin procedure is applied by multiplying the governing equation by a set of appropriate functions and integrating along the contact domain. In this way, by truncating the series at the Nth term, an algebraic system for the series expansion coefficients is obtained and solved by using a suitable normalization condition. This allows to achieve the buckling modes up to an arbitrary amplitude constant. For convenience, in the following the procedure is illustrated for even and odd modes, separately.

3.2. Even modes

In order to investigate the even modes, the second order derivative of the rotation field is expanded in series of Chebyshev polynomials of the first kind, $T_n(\xi)$ with $n \in \mathbb{N}$

$$\varphi''(\xi) = \sum_{n=1}^{\infty} C_{2n-1}T_{2n-1}(\xi), \tag{9}$$

where C_{2n-1} are the unknown coefficients. Higher and lower order derivatives of Eq. (9) can be easily obtained by using relations (31)–(33) provided in the Appendix A.1. Hence, the rotation field and its derivatives involved in the governing Eq. (6) can be written in terms of Chebyshev polynomials of the first and second kinds

$$\varphi'''(\xi) = \sum_{n=1}^{\infty}(2n-1)C_{2n-1}U_{2n-2}(\xi), \tag{10}$$

$$\varphi'(\xi) = \chi_0 + \frac{C_1}{4}T_2(\xi) + \frac{1}{4}\sum_{n=2}^{\infty}C_{2n-1}\left[\frac{T_{2n}(\xi)}{n} - \frac{T_{2n-2}(\xi)}{n-1}\right], \tag{11}$$

[2] Expression (5) for the peel stress follows from the solution of the problem of a rigid punch in frictionless contact with a half-plane (for details, see Muskhelishvili, 2013 p. 492–501) based on the use of complex potentials. As reported in Muskhelishvili (2013), function $\mathcal{K}(t/a)$ assumes different form depending on the presence of sharp or smooth edges of the punch profile. In particular, sharp edges are characterized by a singular pressure distribution, whereas smooth edges imply null pressure at the edge according to Hertz contact theory.

$$\begin{aligned}\varphi(\xi) = \chi_0 T_1(\xi) &+ \frac{C_1}{24}[T_3(\xi) - 3T_1(\xi)] \\ &+ \frac{C_3}{80}[10T_1(\xi) - 5T_3(\xi) + T_5(\xi)] \\ &+ \frac{1}{8}\sum_{n=3}^{\infty} \frac{C_{2n-1}}{n[4(n-2)n^2 + n + 3]} \\ &\times [n(2n+1)T_{2n-3}(\xi) + (2n+1)(3-2n)T_{2n-1}(\xi) \\ &+ (n-1)(2n-3)T_{2n+1}(\xi)], \end{aligned} \tag{12}$$

where χ_0 is an integration constant.

Due to the symmetry properties, it is sufficient to impose the BCs (8) at one edge only. Relations (8) are thus used to obtain the constant χ_0 and the coefficient C_3 in terms of the other unknown coefficients, namely

$$\chi_0 = \frac{1}{4}\left[-C_1 + \frac{C_3}{2} + \sum_{n=3}^{\infty} \frac{C_{2n-1}}{(n-1)n}\right],$$

$$C_3 = C_1 \frac{5}{3} \frac{\tilde{P}(3\rho+1) - 3}{\tilde{P}(1-5\rho) + 5} + 5\sum_{n=3}^{\infty} C_{2n-1} \frac{\tilde{P}\left[\frac{1}{3-4(n-1)n} + \rho\right] - 1}{\tilde{P}(1-5\rho) + 5}.$$

The introduction of the series expansions (9) and (12) into the peeling stress distribution (5) provides

$$q(\xi) = \frac{\overline{E}_h}{2\pi} \frac{1}{\mathcal{K}(\xi)} \sum_{\substack{n=1 \\ n\neq 2}}^{\infty} C_{2n-1} \int_{-1}^{+1} \frac{\mathcal{K}(s)}{s-\xi} q_{2n-1}(s) ds, \tag{13}$$

where functions $q_{2n-1}(s)$ for $n = 1, 3, 4, \dots, \infty$ are listed in Appendix A.2. Depending on the edges function $\mathcal{K}(s)$, relations (34) and (35) for smooth or sharp edges are used to evaluate in closed form the integral in expression (13) (for details see Appendix A.2). As a consequence, the governing Eq. (6) is transformed into an infinite series of Chebyshev polynomials with unknown coefficients C_{2n-1} for $n = 1, 3, 4, \dots, \infty$

$$\sum_{\substack{n=1 \\ n\neq 2}}^{\infty} C_{2n-1} f_{2n-1}(\xi) = 0, \tag{14}$$

where functions $f_{2n-1}(\xi)$, defined in Appendix A.2, are linear combinations of Chebyshev polynomials and depend on the dimensionless axial load $\tilde{P}$ as well as on the governing parameters ρ and κ.

In order to solve the governing Eq. (14) for the unknown coefficients, Eq. (14) is now multiplied by $T_m(\xi)/\sqrt{1-\xi^2}$ or $T_m(\xi)$, with $m = 1, 3, \dots,$ for smooth or sharp edges, respectively, and then integrated for ξ ranging between -1 and 1. Therefore, the following infinite eigensystem is derived in closed form

$$\boldsymbol{A}(\tilde{P})\boldsymbol{c} = \boldsymbol{0}, \tag{15}$$

where $\boldsymbol{c}$ is Chebyshev coefficients vector and $\boldsymbol{A}(\tilde{P})$ is the system coefficient matrix defined in Appendix A.2. Then, the system characteristic Eq. (15), i.e. the buckling spectrum

$$\det[\boldsymbol{A}(\tilde{P})] = 0, \tag{16}$$

provides the eigenvalues $\tilde{P}_i$ for $i = 1, 2, \dots, \infty$, i.e. the dimensionless buckling loads.

Once the eigenvalues are found from Eq. (16), the coefficients C_{2n-1} normalized w.r.t. the first coefficient C_1 are achieved. The displacement field follows by integrating relation (1) and the integration constant is found by imposing $v(\pm 1) = w(\pm 1, 0) = 0$, where $w(x, 0)$ is the vertical displacement of the half-plane surface loaded by the load distribution (13), namely (Muskhelishvili, 2013)

$$w(x, 0) = -\frac{2}{\pi \overline{E}_h} \int_{-a}^{+a} q(t) ln|t - x| \, dt. \tag{17}$$

Table 1
Reference cases: dimensionless governing parameters.

Case	$\rho = \frac{E_b I_b}{G_b A_b^* a^2}$	$\kappa = \frac{\overline{E}_h a^3}{E_b I_b}$
1	0	15.625
2	0	1953
3	0.032	15.625
4	0.0036	1953
5	0	0.125

3.3. Odd modes

As for even modes, the odd modes are investigated by assuming the rotation field second order derivative series expansion of even Chebyshev polynomials as

$$\varphi''(\xi) = \sum_{n=0}^{\infty} C_{2n} T_{2n}(\xi). \tag{18}$$

Relations (31) and (32) in Appendix A.1 provide the derivatives of function $\varphi(\xi)$ up to the third order

$$\varphi'''(\xi) = \sum_{n=0}^{\infty} C_{2n} U_{2n-1}(\xi), \tag{19}$$

$$\varphi'(\xi) = \sum_{n=0}^{\infty} \frac{C_{2n}}{2}\left[\frac{T_{2n-1}(\xi)}{1-2n} + \frac{T_{2n+1}(\xi)}{2n+1}\right], \tag{20}$$

$$\begin{aligned}\varphi(\xi) = \varphi_0 + \frac{1}{24}\Bigg\{ &6C_0 T_2(\xi) - \frac{C_2}{2}[8T_2(\xi) + T_4(\xi)] \\ &+ \sum_{n=2}^{\infty} C_{2n}\left[\frac{3T_{2n-2}(\xi)}{2n^2 - 3n + 1} + \frac{3T_{2n+2}(\xi)}{2n^2 + 3n + 1} - \frac{6T_{2n}(\xi)}{n(4n^2 - 1)}\right]\Bigg\}. \end{aligned} \tag{21}$$

By imposing the BCs (8), the rigid rotation φ_0 and coefficient C_2 can be written as functions of the unknown coefficients C_{2n} for $n = 0, 2, 3, \dots, \infty$, namely

$$\varphi_0 = 3\left(C_0 + \sum_{n=2}^{\infty} \frac{C_{2n}}{1-4n^2}\right),$$

$$C_2 = C_0 \frac{\tilde{P}(64\rho + 3) - 64}{16\tilde{P}} - \sum_{n=2}^{\infty} C_{2n} \frac{64 + \tilde{P}[5 - 64(n^2-1)^2\rho] + n^2[64(n^2-2) + 7\tilde{P}]}{16(4n^4 - 5n^2 + 1)\tilde{P}}.$$

Due to relations (18) and (21), the load term (5) becomes

$$q(\xi) = \frac{\overline{E}_h}{2\pi} \frac{1}{\mathcal{K}(\xi)} \sum_{\substack{n=0 \\ n\neq 1}}^{\infty} C_{2n} \int_{-1}^{1} \frac{\mathcal{K}(s)}{s-\xi} q_{2n}(\xi) ds,$$

where functions $q_{2n}(\xi)$ for $n = 0, 2, 3, \dots, \infty$ are listed in Appendix A.2. Therefore, the governing Eq. (6) assumes the form of an infinite series of Chebyshev polynomials involving the unknown coefficients C_{2n} for $n = 0, 2, 3, \dots, \infty$, as

$$\sum_{\substack{n=0 \\ n\neq 1}}^{\infty} C_{2n} f_{2n}(\xi) = 0, \tag{22}$$

where functions $f_{2n}(\xi)$ for $n = 0, 2, 3, \dots, \infty$ are reported in Appendix A.2.

The solution is achieved by following the same procedure used for the even modes. The system coefficient matrix $\boldsymbol{A}(\tilde{P})$ and the Chebyshev coefficients vector $\boldsymbol{c}$ are reported in Appendix A.2.

Please cite this article as: F.O. Falope, L. Lanzoni and E. Radi, Buckling of a Timoshenko beam bonded to an elastic half-plane: Effects of sharp and smooth beam edges, International Journal of Solids and Structures, https://doi.org/10.1016/j.ijsolstr.2019.08.034

Table 2
Case 1 ($\rho = 0,\ \kappa = 15.625$): dimensionless buckling load p_i and edges effect parameter $\Pi_i = P_{i,Sh}/P_{i,Sm}$. Symbols $^{(o)}$ and $^{(e)}$ denote odd and even modes respectively.

Sharp edges				Smooth edges				
Mode	Present Analysis Series terms, N		Tullini et al. (2013)	Mode	Series terms			Edges effect
	4	5			4	10	12	Π_i
$1^{(e)}$	2.002	∼	2.002	$1^{(e)}$	3.492	3.754	3.728	0.53
$2^{(o)}$	2.321	∼	2.369	$2^{(o)}$	5.137	∼	∼	0.45
$3^{(o)}$	5.023	∼	5.021	$3^{(e)}$	16.155	9.791	9.773	0.51
$4^{(e)}$	9.596	∼	9.594	$4^{(o)}$	18.705	16.540	∼	0.58

Table 3
Case 2 ($\rho = 0,\ \kappa = 1953.13$): dimensionless buckling load p_i and edges effect parameter $\Pi_i = P_{i,Sh}/P_{i,Sm}$. Symbols $^{(o)}$ and $^{(e)}$ denote odd and even modes respectively.

Sharp edges				Smooth edges			
Mode	Present Analysis Series terms, N		Tullini et al. (2013)	Mode	Series terms		Edges effect
	5	10			10	12	Π_i
$1^{(e)}$	52.426	52.112	52.056	$1^{(e)}$	77.138	77.183	0.67
$2^{(o)}$	52.172	∼	52.117	$2^{(o)}$	78.324	∼	0.66
$3^{(o)}$	78.167	∼	78.168	$3^{(o)}$	83.340	83.913	0.93
$4^{(e)}$	80.606	79.513	79.511	$4^{(e)}$	85.839	85.911	0.93

Table 4
Case 3 ($\rho = 0.032,\ \kappa = 15.625$): dimensionless buckling load p_i and edges effect parameter $\Pi_i = P_{i,Sh}/P_{i,Sm}$. Symbols $^{(o)}$ and $^{(e)}$ denote odd and even modes respectively.

Sharp edges				Smooth edges				
Mode	Present Analysis Series terms, N		Tullini et al. (2012)	Mode	Series terms			Edges effect
	4	5			4	10	12	Π_i
$1^{(e)}$	1.918	∼	1.917	$1^{(e)}$	3.300	3.664	∼	0.52
$2^{(o)}$	2.225	∼	2.224	$2^{(o)}$	4.175	∼	∼	0.53
$3^{(o)}$	4.147	∼	4.147	$3^{(e)}$	7.913	6.077	6.051	0.68
$4^{(e)}$	5.863	∼	5.864	$4^{(o)}$	7.999	7.609	∼	0.77

Then, the eigenvalues $\tilde{P}_i$ for $i = 1, 2, \ldots, \infty$ are determined as the roots of the characteristic Eq. (16) and the corresponding eigenvectors $\boldsymbol{c}_i$ are obtained from the non-trivial solution of the homogeneous eigensystem (15) by introducing a suitable normalization w.r.t. the coefficient C_0. Finally, the integration constant corresponding to a rigid body motion is assessed by requiring $v(0) = 0$, according to the skew-symmetry condition of the odd modes.

4. Results and discussion

The eigenvalues determined by solving the characteristic Eq. (16), for both odd and even modes as for sharp and smooth beam edges, are presented and discussed in the present section in terms of the governing dimensionless parameters. Attention is paid to the series expansions convergence. The edge effects on the buckling loads and mode shapes are investigated in detail.

Five reference cases have been considered, whose governing parameters are reported in Table 1.

In order to validate the results provided by the present study, ρ and κ for cases 1 to 4 have been assumed corresponding to the cases numerically investigated in Tullini et al. (2012, 2013). In particular, ρ and κ are related to the governing parameters αL and h/L used in Tullini et al. (2012, 2013) by the following relations:

$$\kappa = (\alpha L)^{\frac{3}{8}}, \quad \rho = \frac{4h}{5L}, \qquad \text{with } L = 2a. \tag{23}$$

Cases 1 and 2 are representative of an E-B beam resting on a compliant and stiff half-plane respectively, whereas cases 3 and 4 simulate a Timoshenko beam on a soft and stiff elastic half-plane respectively. The last case 5 corresponds to an E-B beam resting on a high compliant support. In this limit case, the beam is expected to buckle as a free beam, namely the first buckling load is almost vanishing and the corresponding buckling mode resembles a rigid body rotation. In the following, subscripts $_{Sh}$ and $_{Sm}$ denote a beam with sharp and smooth edges amount, respectively.

The results are reported in terms of the normalized buckling loads

$$p_i = \frac{P_i}{P_E} = \frac{4}{\pi^2}\tilde{P}_i,$$

namely the ith buckling load P_i is normalized w.r.t. the Euler critical load $P_E = \pi^2 E_b I_b / 4a^2$ of a simply supported beam.

In the following, $\Pi_i = P_{i,Sh}/P_{i,Sm}$ will be defined the *edge effect parameter*, being the ratio between the eigenvalues obtained for a beam with sharp and smooth edges corresponding to the same mode number i.

4.1. Buckling loads and modes

The normalized eigenvalues p_i, for $i = 1 \div 4$, are reported in Tables 2–5 for cases 1 to 4. Symbol ∼ denotes the convergence achievement. To be specific, we assume that convergence is at-

Table 5
Case 4 ($\rho = 0.0036$, $\kappa = 1953.13$): dimensionless buckling load p_i and edges effect parameter $\Pi_i = P_{i,Sh}/P_{i,Sm}$. Symbols $^{(o)}$ and $^{(e)}$ denote odd and even modes respectively.

Sharp edges				Smooth edges			
Mode	Present Analysis		Tullini et al. (2012)	Mode	Series terms		Edges effect
	Series terms, N						
	5	10			10	12	Π_i
$1^{(e)}$	46.770	46.362	46.342	$1^{(o)}$	70.181	∼	0.66
$2^{(o)}$	46.416	∼	46.399	$2^{(e)}$	70.267	70.439	0.66
$3^{(e)}$	72.839	70.400	70.400	$3^{(e)}$	72.068	73.705	0.95
$4^{(o)}$	70.776	∼	70.776	$4^{(o)}$	73.134	∼	0.96

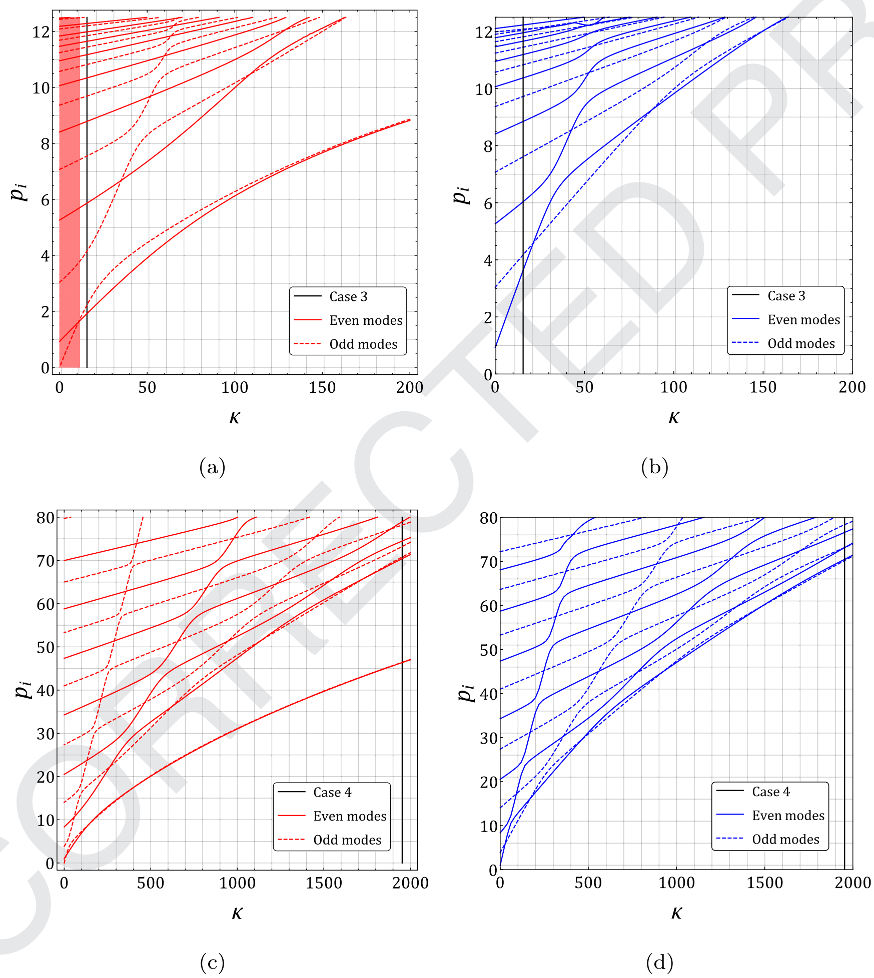

Fig. 3. The stiffness dimensionless parameter $\kappa = \overline{E}_h a^3 / E_b I_b$ influence on the dimensionless buckling loads: even modes (continuous lines) and odd modes (dashed lines). The red background highlights the $\kappa < \kappa_1$ region. (a) Beams with sharp edges: $\rho = 0.032$, low κ values; (b) Beams with smooth edges: $\rho = 0.032$, low κ values; (c) Beams with sharp edges: $\rho = 0.0036$, high κ values; (d) Beams with smooth edges: $\rho = 0.0036$, high κ values. (For interpretation of the references to colour in this figure legend, the reader is referred to the web version of this article.) Q3

tained when the relative error between the solution obtained with N terms and that obtained with $N+1$ terms is lower than 0.1%.

The convergence rate is influenced by the nature of the beam edges, the mode shape and the governing parameters. In particular, the convergence rate is faster for sharp edges than for smooth edges. Indeed, in case of smooth edges, a large number of terms is required for addressing the convergence, with the exception of the second odd mode, as shown in Tables 2–5. In addition, the convergence rate decreases as κ and ρ increase, specially for even modes.

Tables 2 and 4 show that the eigenvalues decrease as the shear parameter ρ increases as well as the stiffness parameter κ decreases. For small values of the parameter κ, the beam shear compliance has no relevant effects on the buckling load and mode. Indeed, in this case the buckling mode resembles a rigid body motion.

Conversely, the edges shape significantly affects the buckling loads, as shown in Tables 2–5 where the first four modes for cases 1÷4 are reported. In particular, for low values of κ (stiff beams on compliant substrates), with special reference to the first mode shape, the parameter κ strongly influences the buckling load. The order in which the mode shape occurs, symmetric or skew, is also influenced by the edges shape. In particular, it can be observed from Tables 2–5 that only case 2 exhibits the same modes sort-

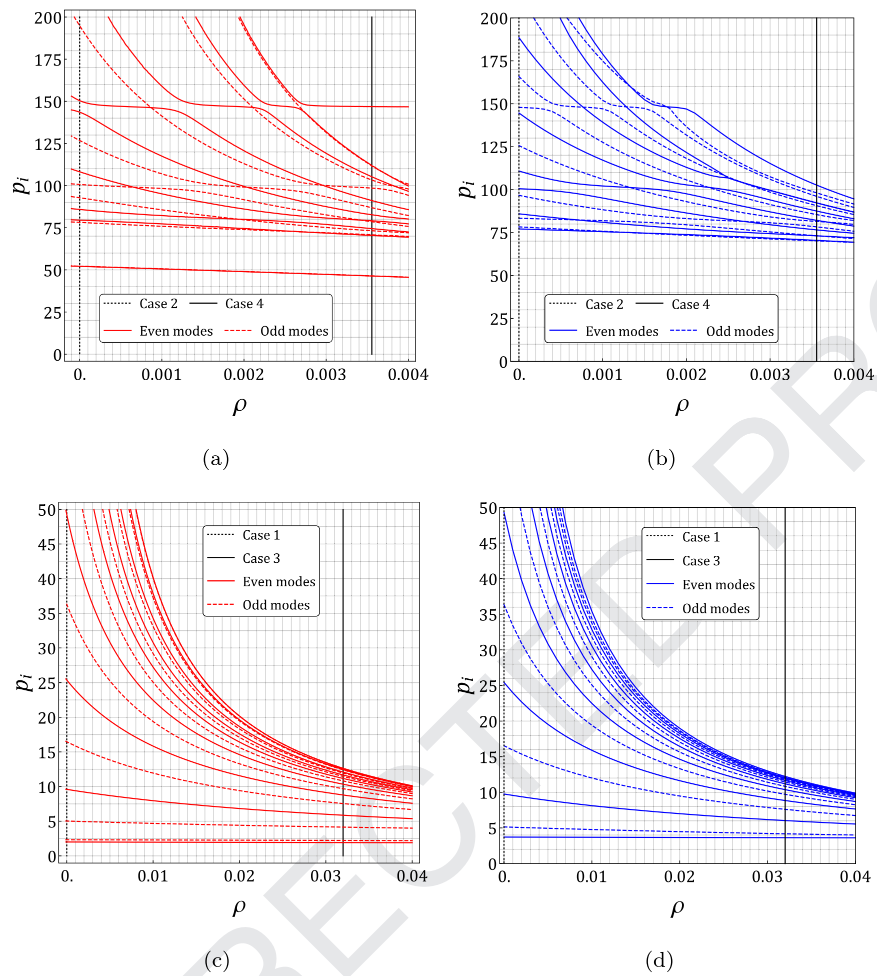

Fig. 4. The shear dimensionless parameter $\rho = E_b I_b / a^2 G_b A_b{}^*$ influence on the dimensionless buckling loads: even modes (continuous lines) and odd modes (dashed lines). (a) Beams with sharp edges: $\kappa = 1953$, low ρ values; (b) Beams with smooth edges: $\kappa = 1953$, low ρ values; (c) Beams with sharp edges: $\kappa = 15.625$, high ρ values; (d) Beams with smooth edges: $\kappa = 15.625$, high ρ values.

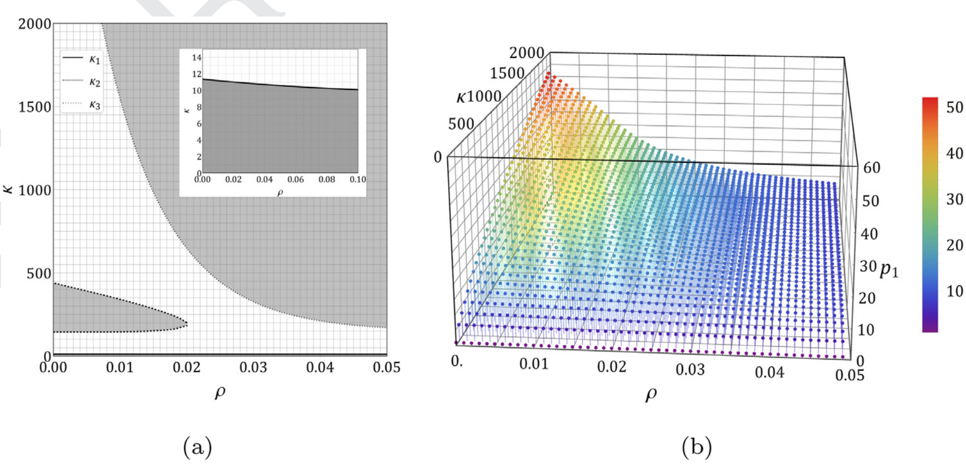

Fig. 5. First critical modes and corresponding buckling loads. (a) Nature of the first critical modes. Grey regions identify the occurrence of odd modes, white regions denote even modes; (b) Dimensionless first critical loads varying the governing parameters κ and ρ.

ing (alternated even and odd modes) both for sharp and smooth edges (symbols (o) or (e) denote odd or even modes, respectively). In all the other cases the mode sorting changes according to the kind of the beam edges.

The effects induced by the governing parameters are shown in Figs. 3 and 4, where the dimensionless buckling loads are plotted varying κ and ρ, for the considered reference cases.

Even and odd modes are plotted in solid and dashed lines, respectively, whereas red and blue lines represent sharp and smooth beam edges, respectively. Vertical black lines denote the reference cases of Table 1.

By comparing Fig. 3(a) and (c) for beams with sharp edges, with Fig. 3(c) and (d) concerning beams with smooth edges, a switch between even and odd modes is observed. In particular,

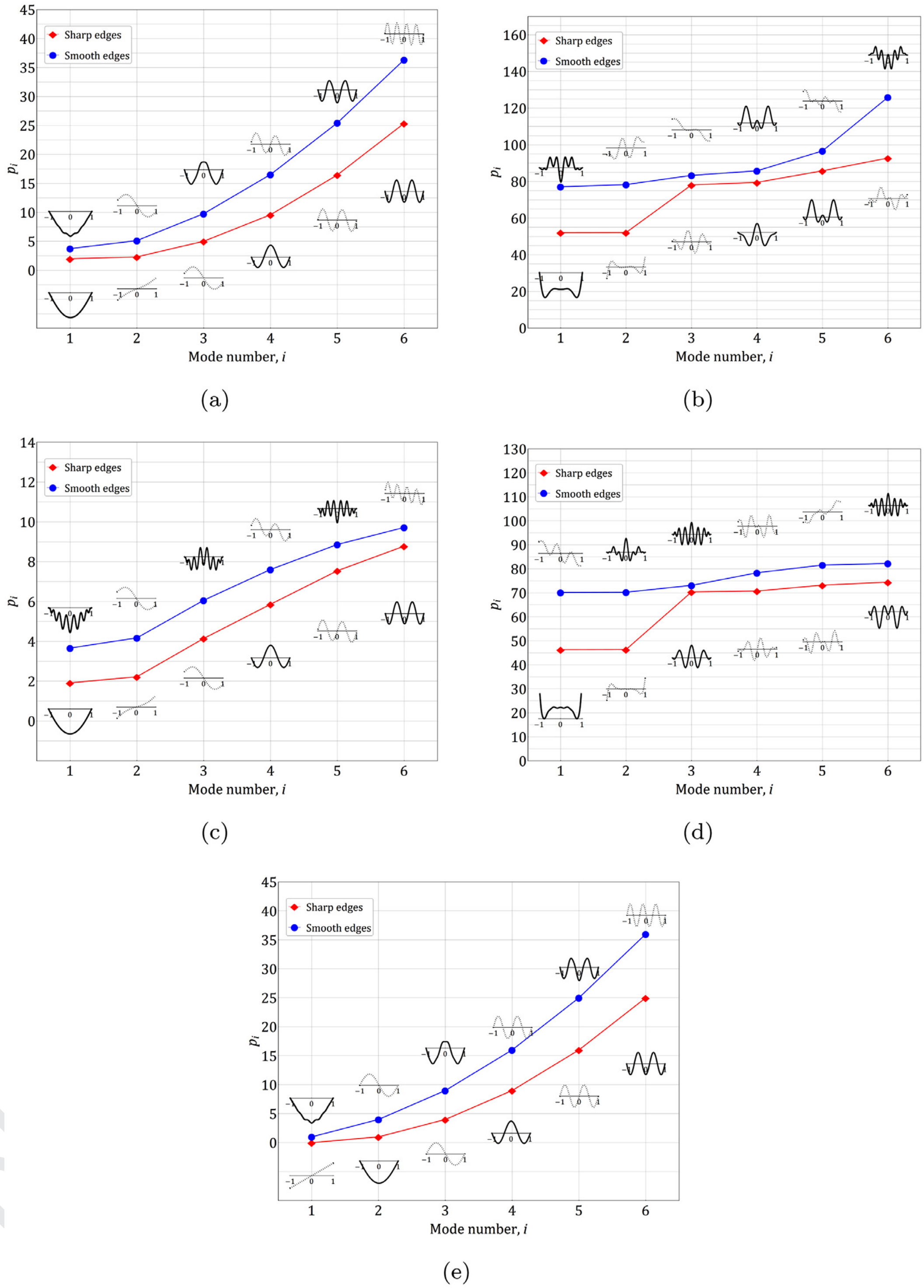

Fig. 6. Dimensionless buckling loads and associated buckling modes. (a) Case 1; (b) Case 2; (c) Case 3; (d) Case 4; (e) Case 5 (vanishing half-plane).

both for odd or even modes, the curves behave smoothly everywhere except where they approached each other. Therein, instead of continuing smoothly and crossing, they suddenly deviate and do not intersect. Such a behaviour is known as *veering* phenomenon (Mace and Manconi, 2012). Conversely, the intersection points between even and odd modes, denote the occurring of simultaneous even and odd modes under the same buckling load. The values of κ corresponding to the intersection between the first odd and even modes will be denoted as κ_i. In particular, for a given value of the shear compliance ρ, the smallest value of κ_i will be denoted by κ_1.

Making reference to case 3, for beams with sharp edges we found $\kappa_1 \cong 11.53$, as shown in Fig. 3(a). Therefore, for $\kappa < \kappa_1$ (compliant half-plane) the first buckling mode is odd and close to a

Please cite this article as: F.O. Falope, L. Lanzoni and E. Radi, Buckling of a Timoshenko beam bonded to an elastic half-plane: Effects of sharp and smooth beam edges, International Journal of Solids and Structures, https://doi.org/10.1016/j.ijsolstr.2019.08.034

rigid rotation, whereas for $\kappa_1 < \kappa < \kappa_2$ the first buckling mode is even. Note also that for beams with smooth edges we obtained $\kappa_1 \cong 21.4$.

The buckling loads variation with the shear parameter ρ are reported in Fig. 4(a)–(d). For low values of ρ and high value of κ the veering phenomenon can be observed both for beams with sharp and smooth edges, as shown in Fig. 4(a) and (b), respectively. As the parameter ρ grows, the buckling loads and modes tend to approach each others, with special reference to higher modes, as shown in Fig. 4(c) and (d). Note also that the lowest even and odd modes are almost unaffected by the parameter ρ, as confirmed by the results listed in Tables 2–5.

The buckling modes and loads of beams with sharp edges are represented in Fig. 5(a) and (b), respectively, varying both the parameters ρ and κ. In particular, for any couple of $\kappa - \rho$ values, grey or white regions of Fig. 5(a) characterize systems for which the first critical load is an odd or even mode, respectively. The detail in Fig. 5(a) shows that for $\rho < 0.1$, which is relevant for practical cases, the first buckling mode is always odd for $\kappa < 10$. Furthermore, the same detail emphasizes the negligible dependence of the first critical load p_1 on the shear parameter ρ for low values of κ.

The dimensionless plot of Fig. 5(b) provides the first buckling load p_1 as a function of the problem governing parameters. This plot highlights that the first critical loads are almost independent of the shear parameter ρ for low values of κ.

The first six buckling loads and modes corresponding to the considered reference cases are reported in detail in Fig. 6. In particular, Fig. 6(c) and (d) show that the buckling modes of beams with smooth edges involve a larger wave number and higher buckling loads than beams with sharp edges.

Therefore, Fig. 6 together with the edge effect parameter $\Pi_i = P_{i,Sh}/P_{i,Sm}$, provided in Tables 2–5, always show that beams with smooth edges display higher buckling loads w.r.t. beams with sharp edges. Indeed, the edge effect parameter ranges between $0.5 \le \Pi \le 1$ and, referred to Fig. 6, the buckling loads curves of beams with smooth edges lay over the curves of beams with smooth edges for all the reference cases. Such a difference is more evident for cases 1 and 3 and for the first modes, for which a beam with smooth edges exhibits a critical load almost double of that of a beam with sharp edges.

A rigid-body like buckling mode does not occur for beams with smooth edges resting on a high compliant half-plane (see Fig. 6(e)). Conversely, Fig. 6(c) shows that beams with sharp edges resting on a high compliant half-plane exhibit a first odd buckling mode close to a rigid rotation. Such a trend is not observed for case 3, despite of the high compliance of the half-plane, $\rho = 0.032$. For such a situation it is worth noticing that the buckling loads of beams with sharp and smooth edges tend to coincide as the mode number increases, accordingly to Fig. 4. Note also that when the half-plane stiffness is lower (cases 1, 5), the buckling loads approach those of an E-B simply supported beam, namely $p_i \approx n^2$.

4.2. Rigid beam resting on a compliant half-plane

The first buckling load of a rigid beam resting on a compliant substrate, namely as $\kappa \longrightarrow 0^+$, is investigated in the present Section.

Looking for the solution of the governing Eq. (6) as a constant term ϕ_0, the only non-vanishing term turns out to be the load contribute (5)[3], namely

$$q(\xi) = \begin{cases} \frac{\bar{E}_h\phi_0}{2\pi} \frac{1}{\sqrt{1-\xi^2}} \int_{-1}^{+1} \frac{\sqrt{1-s^2}}{s-\xi}\, ds, & \text{for sharp edges,} \\ \frac{\bar{E}_h\phi_0}{2\pi} \sqrt{1-\xi^2} \int_{-1}^{+1} \frac{ds}{(s-\xi)\sqrt{1-s^2}}, & \text{for smooth edges.} \end{cases} \tag{24}$$

[3] The identities $T_0(\xi) = U_0(\xi) = 1$ are used in (24).

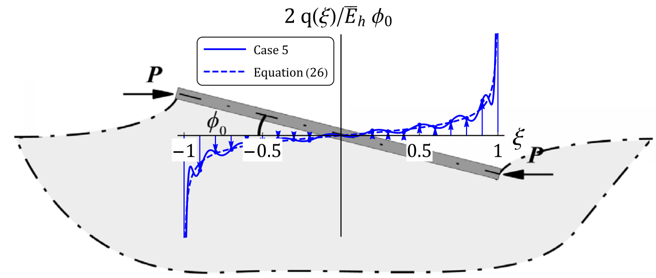

Fig. 7. Case 5: First mode pressure distribution. Series solution (solid line) vs closed form solution (dashed line).

However, by using Eq. (34) the pressure distribution (24) for beams with smooth edges is zero. Therefore, the moment generated by the axial loads P as a consequence of a rigid rotation ϕ_0 of the beam, namely

$$M_0 = 2\phi_0 P a, \tag{25}$$

cannot be balanced by the soil reaction, except for $P = 0$, namely only the trivial solution is admitted. A rigid-like buckling mode cannot occur for beams with smooth edges.

Conversely, the peeling stress distribution (24) at the beam ends is singular for beams with sharp edges and, based on identity (35), it reads

$$q_{Sh}(\xi) = -\frac{\bar{E}_h\phi_0}{2}\frac{\xi}{\sqrt{1-\xi^2}}. \tag{26}$$

Therefore, a square-root singular pressure, in agreement with Lanzoni and Radi (2016), takes place at the beam sharp edges and it can balance the external moment originated by the axial load P as a consequence of the rigid rotation ϕ_0 of the beam. A sketch of such a configuration is found in Fig. 7, where the dashed line denotes the singular pressure distribution (26) whereas the solid line represents the pressure distribution obtained for the case 5. Both solutions have been normalized by $\phi_0\bar{E}_h/2$.

On the other hand, the overall moment generated by the pressure distribution (26) turns out to be

$$M_0 = 2a^2\int_0^1 q(\xi)\xi\, d\xi = \frac{\pi\bar{E}_h\phi_0 a^2}{4}. \tag{27}$$

Moreover, by comparing Eqs. (25) and (27) the following relation between the overall moment and the rigid rotation is found

$$\phi_0 = \frac{4M_0}{\bar{E}_h\pi a^2},$$

in agreement with the well known Galin solution for a rigid flat punch resting on an elastic half-plane and subject to a couple M_0 Kachanov et al. (2013).

A useful analytic design formula for the first buckling load, which holds for small values of κ, is provided by comparing (25) with (27), namely

$$P_{cr}^{(o)} \approx \frac{\bar{E}_h a\pi}{8} \text{ or } p_{cr}^{(o)} \approx \frac{\kappa}{2\pi}, \qquad \text{for } \kappa < \kappa_1. \tag{28}$$

In particular, for case 5 ($\kappa = 0.125$ and $\rho = 0$), the design formula (28) provides a buckling load $p_{cr}^{(o)} = 0.198$, with a relative error lower than 0.34% w.r.t. the provided series solution. Therefore, Eq. (28) can be used to predict the buckling loads of rigid beams resting on compliant substrates, i.e. for $\kappa < \kappa_1$.

4.3. Beam resting on a Winkler soil

The dimensionless buckling loads of an E-B beam resting on a Winkler soil (WS) are reported in Fig. 8(a) varying the WS di-

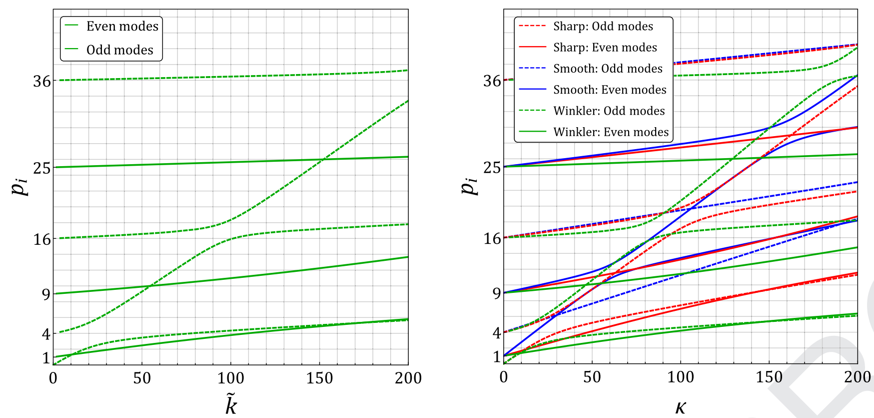

(a) (b)

Fig. 8. (a) Dimensionless buckling loads of an E-B beam resting on a Winkler soil varying the parameter $\tilde{k} = ka^4/E_bI_b$; (b) Critical loads of an E-B beam supported by the Winkler soil compared with those of an E-B beam resting on an elastic half-plane by assuming $\tilde{k} = 3\pi\kappa/8$ according to Eq. (30).

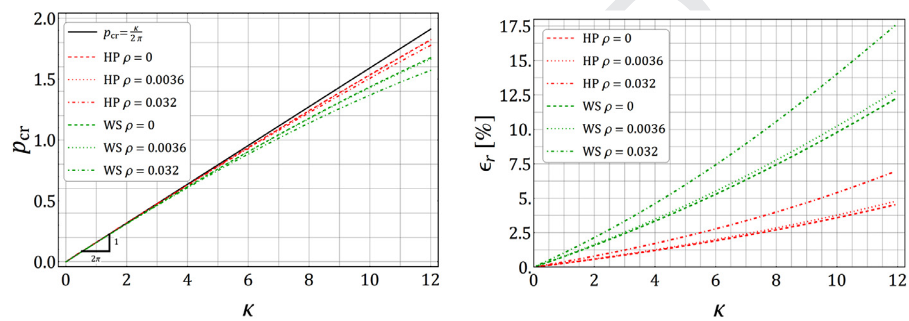

(a) (b)

Fig. 9. (a) Dimensionless buckling loads p_{cr} predicted by Eq. (28) compared with the buckling loads of beams with sharp edges resting on a half-plane (HP) and on Winkler soil (WS) for different values of ρ; (b) relative errors $\varepsilon_r = 1 - P_1/P_{cr}^{(o)}$ between Eq. (28) and the exact solution varying the parameter κ. (For interpretation of the references to color in the text, the reader is referred to the web version of this article.)

mensionless parameter $\tilde{k} = ka^4/E_bI_b$, being k the Winkler constant Hetényi (1971). As expected, as $k \to 0^+$ the critical loads resemble those of a simply supported E-B beam ($p_i \approx n^2$). It is worth noticing that, similarly to the case of beams resting on a half-plane, the veering phenomenon occurs also for beams resting on a local soil. In particular, the trend of the first odd mode curve in Fig. 8(a) is close to that displayed in Fig. 3(a) concerning beams with sharp edges, both in terms of buckling loads and sorting of even-odd modes. This analogy is confirmed by Fig. 8(a), where the curves of Fig. 8(a) have been expressed w.r.t the half-plane problem governing parameter κ and compared with the E-B beam bonded to an elastic half-plane dimensionless buckling load[4] Note that, for all the observed values of κ, the slope of the curves representative of beams with smooth edges are always greater than those of beams with sharp edges, which in turn are greater than those of beams supported by a WS. Therefore, it seems that beams supported by a WS subjected to buckling exhibit a softer buckling behaviour w.r.t. beams resting on a half-plane. However it should be remarked that the governing parameter $\tilde{k}$ differs from the stiffness parameter κ of a beam resting on an elastic half-plane. Indeed, in order to make a comparison between the results provided by the present approach for a beam on an elastic half-plane and those provided by the simplest WS assumption (as reported in Fig. 8(a)), it becomes necessary to define a relation between the Winkler constant k and the half-plane elastic modulus $\overline{E}_h$. With this aim, the first buckling load obtained from the two substrate models are compared to obtain the required relation.

To be specific, for rigid beams resting on compliant substrates, in particular for $\kappa < \kappa_1$, a straightforward relation can be established between the Winkler constant k and the half-plane elastic modulus $\overline{E}_h$. Let us consider a flat punch on a WS subjected to a rotation ϕ_0 around its centre. Then, the interfacial pressure distribution assumes the form

$$q_{WS}(\xi) = -k\phi_0\xi a,$$

which implies an external moment M_0 given by

$$M_0 = \frac{2}{3}k\phi_0 a^3. \qquad (29)$$

Thus, by comparing Eqs. (27) and (29), the following relation between the half-plane generalized Young modulus and the WS constant k holds

$$k = \frac{3\overline{E}_h}{8a}\pi, \qquad \tilde{k} = \frac{3}{8}\pi\kappa. \qquad (30)$$

Therefore, the buckling load of a rigid beam resting on a WS, which depends on the WS constant k Hetényi (1971), can be expressed as a function of the dimensionless stiffness parameter κ by using relation $(30)_2$.

Fig. 9 (a) shows the buckling loads of a beam resting on a WS (Hetényi, 1971) by using relation $(30)_2$ (green lines) and the buck-

[4] In order to properly compared the WS buckling curves with those of a beam resting on a half-plane model, a relation between the half-plane elastic modulus and the Winkler constant, Eq. (30) will be provided in the present section.

ling load of beams with sharp edges resting on a half-plane (red lines).[5]

As expected, formula (28) predicts reasonably well the first bulking load for low values of κ, as shown in Fig. 9(a). The discrepancy between formula (28) and the effective first buckling load increases as κ and ρ increase, as reported in Fig. 9(b) where the relative errors are shown reported. However, Fig. 9(b) shows that for $\kappa < 12$, the relative error is lower than 20%, also for high values of the shear parameter ρ. An alternative relation between the soil constant k and the half-plane elastic modulus $\overline{E}_h$ can be found in Biot (1937).

5. Conclusion

The buckling analysis of a compressed Timoshenko beam with sharp or smooth edges in bilateral and frictionless contact with an elastic half-plane has been investigated. By expanding the rotation field of the beam cross sections in series of Chebyshev polynomials of the first kind, the governing integro-differential equation has been transformed into an eigenvalue problem. This approach has provided both the buckling loads and mode shapes as function of the governing problem parameters, κ and ρ, the beam flexural compliance compared to the half-plane stiffness and the ratio between the beam bending stiffness and its shear stiffness, respectively. Five reference cases have been investigated in detail, and the obtained results have been compared with those available in the Literature, founding good agreement.

The influence of the stiffness parameter κ on the buckling load is more relevant than the shear parameter ρ influence. Moreover, the dependence of the buckling loads on the shear compliance is more pronounced on the higher modes. It is worth noticing that parameter κ affects also the sorting of the even or odd critical modes.

It has been shown that beams with smooth edges can not exhibit rigid-body like modes. Conversely, for beams with sharp edges a particular value of the parameter κ, called κ_1, has been interpreted as a soil stiffness threshold for the occurrence of a rigid-like mode. Indeed, for $\kappa < \kappa_1$ the first system buckling mode is odd and closer to a rigid body rotation. On the other hand it has been shown that for $\rho < 0.1$, the first mode exhibited by stiff beams on compliant supports ($\kappa < 9$) is always odd.

A simple relation to predict the buckling loads of beams on compliant substrate has been proposed also. In agreement with the Galin solution for the rigid punch, a straightforward relation between the Winkler soil constant and the half-plane elastic modulus holding for rigid beams has been found.

The dimensionless curves of Fig. 5 have been provided as a useful design tool for the critical load evaluation.

The performed results can be used as a reliable support for the design of layered systems characterized by high length-to-thickness ratios, for which the instability phenomena represent the main task. The challenging problem of a compressed beam in frictional contact with an underlying elastic support will be handled in a future work.

Acknowledgements

Financial support from the Italian Ministry of Education, University and Research (MIUR) in the framework of the Project PRIN 2017 *Modelling of constitutive laws for traditional and innovative building materials* (code 2017HFPKZY) is gratefully acknowledged. Authors also acknowledge INdAM-GNFM "Gruppo Nazionale di Fisica Matematica".

[5] It is remarked that Eq. $(30)_1$ provides a relation between the half-plane modulus and the WS constant based on the rigid beam assumption. Therefore, relation $(30)_1$ does not involve the parameters κ and ρ.

Please cite this article as: F.O. Falope, L. Lanzoni and E. Radi, Buckling of a Timoshenko beam bonded to an elastic half-plane: Effects of sharp and smooth beam edges, International Journal of Solids and Structures, https://doi.org/10.1016/j.ijsolstr.2019.08.034

Appendix A

A1. Integral formulae involving Chebyshev polynomials

The Chebyshev polynomials $T_n(x)$ and $U_n(x)$ of first and second kinds of order n are defined through the following identities

$$T_n(x) = \cos[n \arccos(x)],$$
$$U_n(x) = \frac{\sin[(n+1)\arccos(x)]}{\sin[\arccos(x)]},$$

with $0 \le \arccos(x) \le \pi$. The following relations of Chebyshev polynomials in the interval $[-1, 1]$ (Mason and Handscomb, 2002) have been used:

$$T_n'(\xi) = n\, U_{n-1}(\xi), \tag{31}$$

$$\int T_n(x)\, dx = \begin{cases} \dfrac{1}{2}\left[\dfrac{T_{n+1}(x)}{n+1} - \dfrac{T_{|n-1|}(x)}{n-1}\right], & n \ne 1 \\ \dfrac{1}{4} T_2(x), & n = 1 \end{cases}, \tag{32}$$

$$T_n(\xi) = \frac{1}{2}[U_n(\xi) - U_{n-2}(\xi)] \tag{33}$$

$$\int_{-1}^{1} \frac{T_n(x)}{\sqrt{1-x^2}(x-y)}\, dx = \mathrm{sign}(n)\, \pi\, U_{n-1}(y), \tag{34}$$

$$\int_{-1}^{1} \frac{\sqrt{1-x^2}\, U_n(x)}{x-y}\, dx = \begin{cases} \pi\, T_{n+1}(y), & \text{for } n \le -2 \\ -\pi\, T_{n+1}(y), & \text{for } n > -2 \\ 0. & n = -1 \end{cases}, \tag{35}$$

A2. Problem known function and coefficient matrices

The term involving the peeling stress $q(\xi)$ in the governing Eq. (6) can be decomposed as

$$q(\xi) = \frac{\kappa}{2\pi} \frac{1}{\mathcal{K}(\xi)} \int_{-1}^{+1} \frac{\mathcal{K}(s)}{s-\xi} \begin{cases} \sum_{\substack{n=1 \\ n\ne 2}}^{\infty} C_{2n-1}\, q_{2n-1}(s)\, ds, & \text{even modes} \\ \sum_{\substack{n=0 \\ n\ne 1}}^{\infty} C_{2n}\, q_{2n}(s)\, ds, & \text{odd modes} \end{cases} \tag{36}$$

where the introduced functions $q_i(s)$ turn out to be

$$q_1(s) = \frac{s}{3(\tilde{P}+5\omega)}\left\{3[\omega(20\rho+9)-4] - \tilde{P} + s^2 \frac{\tilde{P} - 15\omega(2\rho+1) + 10}{2} + s^4(3\omega - \tilde{P})\right\},$$

$$q_{2n-1}(s) = s\left\{\frac{\tilde{P}[6n(n-1)(10\rho+1)+3] + 5\omega(2n-3)(2n+1)[2(n-1)n(6\rho+1)-1]}{4n\{n[4n(n-2)+1]+3\}(\tilde{P}+5\omega)}\right.$$
$$\left. + s^2 \frac{5(8\rho+1)[\tilde{P} + \omega(2n-3)(2n+1)]}{2(3-2n)(2n+1)(\tilde{P}+5\omega)} + \frac{s^4}{5}\left[\frac{4(n-2)(n+1)\tilde{P}}{(3-2n)(2n+1)(\tilde{P}+5\omega)} + 1\right]\right\}$$
$$+ \frac{1}{8}\left\{\frac{T_{2n-3}(s)}{n(5-2n)-3} - \frac{T_{2n+1}(s)}{n(2n^2+1)} + \left[\frac{1}{n(n-1)} + \rho\right] T_{2n-1}(s)\right\},$$

$$q_0(s) = \frac{4(3\omega-1) - \tilde{P}}{2\tilde{P}} + (6\rho+1)s^2 - \frac{s^4}{2},$$

$$q_{2n}(s) = 4n^2[\tilde{P} + \omega(4n^2-11) + 3] - \tilde{P} + 4(7\omega-3) + s^2\Big[6(1-n^2)(4\rho+1)\tilde{P}$$
$$+ 2s^2\tilde{P}(n^2-1)\Big] + \frac{T_{2n}(s)(n^2-1)[2\rho(4n^2-1)+1]}{2[n^2(4n^2-5)+1]}$$
$$+ \frac{T_{2n+2}(s)(1-n)(2n-1) - T_{2n-2}(s)(n+1)(2n+1)}{8[n^2(4n^2-5)+1]},$$

being $\omega = 1 - \tilde{P}\rho$. Therefore, based on relations (34) and (35), the governing integro-differential Eq. (6) is expressed in an infinite series form

$$\begin{matrix} \sum_{\substack{n=1 \\ n\ne 2}}^{\infty} C_{2n-1} f_{2n-1}(\xi) = 0, & \text{for even modes} \\ \sum_{\substack{n=0 \\ n\ne 1}}^{\infty} C_{2n} f_{2n}(\xi) = 0, & \text{for odd modes} \end{matrix} \tag{37}$$

where functions $f_1(\xi)$ and $f_{2n-1}(\xi)$ assume the following expressions for sharp or smooth beam edges

Please cite this article as: F.O. Falope, L. Lanzoni and E. Radi, Buckling of a Timoshenko beam bonded to an elastic half-plane: Effects of sharp and smooth beam edges, International Journal of Solids and Structures, https://doi.org/10.1016/j.ijsolstr.2019.08.034

$$
\begin{aligned}
f_1(\xi) = {} & \frac{1}{192(\tilde{P}+5\omega)}\left\{\frac{2\kappa\left[-5\tilde{P}\left(72\rho^2+1\right)+8(45\rho-7)+159\omega\right]}{\sqrt{1-\xi^2}}\right. \\
& \left. +8\{(15\rho(24\rho+13)+8)\tilde{P}^2-3(7\omega+65)\tilde{P}+120[\omega(\omega+6)-3]\}\right\}, \quad \text{for sharp edges,}
\end{aligned}
$$

$$
\begin{aligned}
f_1(\xi) = {} & \frac{48[9\tilde{P}+20(1-2\omega)]-16[\rho(60\rho+27)+1]\tilde{P}^2+\kappa\sqrt{1-\xi^2}[3(80\rho^2+1)\tilde{P}-15(16\rho-7)\omega+16]}{48(\tilde{P}+5\omega)} \\
& -\xi^2\left\{\frac{\kappa\sqrt{1-\xi^2}\{40(3\rho-1)+3[19\omega-1\tilde{P}(40\rho^2+1)]\}-60[(5-\omega)\tilde{P}+12(2\omega+1)]}{12(\tilde{P}+5\omega)}\right. \\
& \left.+\tilde{P}^2\frac{5\rho(12\rho+5)+2}{\tilde{P}+5\omega}\right\}+\xi^4\frac{\kappa\sqrt{1-\xi^2}(3\omega-\tilde{P})+10\tilde{P}(\tilde{P}-3\omega)}{6(\tilde{P}+5\omega)}, \quad \text{for smooth edges,}
\end{aligned}
$$

$$
\begin{aligned}
f_{2n-1}(\xi) = {} & \kappa\left\{\frac{\tilde{P}[4n(n-84\omega)+3]+4n\{10[4(n-2)n^2+n+3]\rho\omega+n[8(n-2)n-13]\omega+10(n-1)\}+15\omega}{16n[4(n-2)n^2+n+3]\sqrt{1-\xi^2}(\tilde{P}+5\omega)}\right. \\
& \left.+\xi^4\frac{[\tilde{P}+(2n-3)(2n+1)\omega][\kappa(20\rho+3)-10\sqrt{1-\xi^2}\tilde{P}]}{2(2n-3)(2n+1)\sqrt{1-\xi^2}(\tilde{P}+5\omega)}+\xi^6\frac{\kappa[\tilde{P}+(2n-3)(2n+1)\omega]}{2(3-2n)(2n+1)\sqrt{1-\xi^2}(\tilde{P}+5\omega)}\right\} \\
& +\sqrt{1-\xi^2}\left\{\frac{-3\tilde{P}(\tilde{P}+5\omega)-2n[-3(30\rho^2+1)\tilde{P}^2+55\omega\tilde{P}-180\omega+90]}{4n[4(n-2)n^2+n+3]\sqrt{1-\xi^2}(\tilde{P}+5\omega)}\right. \\
& \left.+n^2\frac{2[-3(70\rho^2+1)\tilde{P}^2+35\omega\tilde{P}+60\omega(4\omega-7)+210]+80n\omega(\tilde{P}-6\omega)+40n^2\omega(6\omega-\tilde{P})}{4n[4(n-2)n^2+n+3]\sqrt{1-\xi^2}(\tilde{P}+5\omega)}\right\} \\
& +U_{2n}(\xi)\frac{8(n-1)(2n+1)\sqrt{1-\xi^2}\tilde{P}+\kappa+8\kappa n\left(-2n^2+n+1\right)\rho-4\kappa n}{64(n-1)n(2n+1)\sqrt{1-\xi^2}} \\
& +\frac{\kappa U_{2(n+1)}(\xi)}{64n(2n+1)\sqrt{1-\xi^2}}+\frac{U_{2(n-1)}(\xi)}{64}\left[\kappa\frac{8n(2n-3)\rho+3}{n(2n-3)\sqrt{1-\xi^2}}-\frac{8\tilde{P}}{n-1}\right] \\
& +\frac{U_{2(n-2)}(\xi)}{64(n-1)(2n+1)}\left[8\left(1-2n+\frac{1}{n}\right)\tilde{P}+\kappa\frac{8(n-1)(2n+1)\rho+3}{\sqrt{1-\xi^2}}\right] \\
& +\frac{\kappa U_{2(n-3)}(\xi)}{64[n(2n-5)+3]\sqrt{1-\xi^2}}, \quad \text{for sharp edges,}
\end{aligned}
$$

$$
\begin{aligned}
f_{2n-1}(\xi) = {} & \frac{-5\{2(n-1)n[4(n-1)n-11]+3\}\omega\tilde{P}+[6(1-n)n-3]\tilde{P}^2+60n[4(n-2)n^2+n+3]\omega^2}{4n[4(n-2)n^2+n+3](\tilde{P}+5\omega)} \\
& +\kappa\sqrt{1-\xi^2}\frac{[5(n-1)n+6]\tilde{P}+(n-1)n\{\omega[4(n-1)n(40\rho+13)-120\rho-119]+40\}+30\omega}{16n[4(n-2)n^2+n+3](\tilde{P}+5\omega)} \\
& +\xi^2\frac{[\tilde{P}+(2n-3)(2n+1)\omega][120\omega-15\tilde{P}+2\kappa\sqrt{1-\xi^2}(10\rho+1)]}{2(3-2n)(2n+1)(\tilde{P}+5\omega)} \\
& +\xi^4\frac{[\tilde{P}+(2n-3)(2n+1)\omega](\kappa\sqrt{1-\xi^2}-10\tilde{P})}{2(2n-3)(2n+1)(\tilde{P}+5\omega)} \\
& +U_{2(n-1)}(\xi)\frac{\tilde{P}\{2-4n[8n(n-1)\rho+1]\}+\kappa\sqrt{1-\xi^2}+8n(n-1)(\kappa\sqrt{1-\xi^2}\rho+4n-2\omega)}{16n(n-1)} \\
& +\frac{U_{2n}(\xi)}{32n}\left(4\tilde{P}-\frac{2\kappa\sqrt{1-\xi^2}}{2n+1}\right)+U_{2(n-2)}(\xi)\frac{2(2n-3)\tilde{P}-\kappa\sqrt{1-\xi^2}}{16[n(2n-5)+3]}, \quad \text{for smooth edges,}
\end{aligned}
$$

$$
\begin{aligned}
f_0(\xi) = {} & \xi\left[\kappa\frac{3\tilde{P}(48\rho+5)-64}{32\sqrt{1-\xi^2}}-2(\tilde{P}-6\omega)\right]+\xi^3\left[2\tilde{P}-\frac{\kappa(24\rho+5)}{8\sqrt{1-\xi^2}}\right] \\
& +\frac{\kappa\xi^5}{4\sqrt{1-\xi^2}}, \quad \text{for sharp edges,}
\end{aligned}
$$

$$
f_0(\xi) = \frac{\xi}{8}[16(\xi^2-1)\tilde{P}+\kappa\sqrt{1-\xi^2}(3-2\xi^2+24\rho)+96\omega], \quad \text{for smooth edges,}
$$

$$
\begin{aligned}
f_{2n}(\xi) = {} & \frac{\xi}{32(4n^2-1)}\left\{\frac{\kappa\left\{(32(4-5n^2)\rho\tilde{P}+n^2[64[\omega(1-n^2)+1]-27\tilde{P}]+15\tilde{P}-32(\omega+1)\right\}}{(n^2-1)\sqrt{1-\xi^2}\tilde{P}}\right.\\
& \left.+96(\tilde{P}-4\omega)\right\}+\frac{\xi^3}{8(1-4n^2)}\left(16\tilde{P}-\kappa\frac{24\rho+7}{\sqrt{1-\xi^2}}\right)+\frac{\kappa\xi^5}{(4-16n^2)\sqrt{1-\xi^2}}\\
& +T_{2n-1}(\xi)\frac{\kappa(2n-1)\{8[n(2n-1)-1]\rho+3\}+16[n(1-2n)+1]\sqrt{1-\xi^2}\tilde{P}}{32(1-n)(1-4n^2)\sqrt{1-\xi^2}}\\
& +T_{2n+1}(\xi)\frac{16[n(2n+1)-1]\sqrt{1-\xi^2}\tilde{P}-\kappa(2n+1)\{8[n(2n+1)-1]\rho+3\}}{32(1+n)(4n^2-1)\sqrt{1-\xi^2}}\\
& +\frac{\kappa}{32\sqrt{1-\xi^2}}\left[\frac{T_{2n+3}(\xi)}{n(2n+3)+1}+\frac{T_{2n-3}(\xi)}{n(2n-3)+1}\right]+2n\omega U_{2n-1}(\xi),\ \text{for sharp edges,}\\
f_{2n}(\xi) = {} & \xi\frac{4(9-8\xi^2)\tilde{P}+\kappa\sqrt{1-\xi^2}[2(\xi^2-12)\rho-5]-96\omega}{8(4n^2-1)}+\frac{\tilde{P}}{2}\left[\frac{T_{2n-1}(\xi)}{1-2n}\ \frac{T_{2n+1}(\xi)}{1+2n}\right]\\
& +U_{2n-1}(\xi)\frac{4n[8\omega n^2-(\tilde{P}+2\omega)]+\kappa\sqrt{1-\xi^2}[1+2\rho(4n^2-1)]}{4(n^2-1)}\\
& +\frac{4\tilde{P}(n-1)-\kappa\sqrt{1-\xi^2}}{16}\left[\frac{U_{2n-3}(\xi)}{n(2n-3)+1}+\frac{U_{2n+1}(\xi)}{n(2n+3)+1}\right],\ \text{for smooth edges.}
\end{aligned}
$$

In order to remove the spatial variable dependences from the series governing Eq. (37), it is multiplied by $T_m(\xi)/\sqrt{1-\xi^2}$ or $T_m(\xi)$ (with $m \in \mathbb{N}$) for sharp and smooth beam edges, respectively, and then integrated over the contact domain. By using results (44) and (45) leads to obtain the following eigensystem problem

$$\boldsymbol{A}(\tilde{P})\boldsymbol{c} = \boldsymbol{0}. \tag{38}$$

being

$$\boldsymbol{A}(\tilde{P}) = \begin{cases} \left[\boldsymbol{f}_m(\tilde{P}) \mid \boldsymbol{F}_{m,2n-1}(\tilde{P})\right], & \text{for even modes} \\ \left[\boldsymbol{g}_m(\tilde{P}) \mid \boldsymbol{G}_{m,2n}(\tilde{P})\right], & \text{for odd modes} \end{cases} \tag{39}$$

the system coefficients matrix and $\boldsymbol{c}$ the Chebyshev coefficients vector. The symbol | denotes concatenation. In particular, the coefficients f_m, $F_{m,2n-1}$, g_m and $G_{m,2n}$ read

$$f_m = \boldsymbol{f}_1(\tilde{P})\cdot\boldsymbol{t}_{m\ Even}, \quad F_{m,2n-1} = \boldsymbol{f}_{2n-1}(\tilde{P})\cdot\boldsymbol{t}_{m\ Even}, \tag{40}$$

$$g_m = \boldsymbol{g}_0(\tilde{P})\cdot\boldsymbol{t}_{m\ Odd}, \quad G_{m,2n} = \boldsymbol{g}_{2n}(\tilde{P})\cdot\boldsymbol{t}_{m\ Odd}, \tag{41}$$

being: For sharp edges:

$$
\boldsymbol{t}_{m\ Even} = \begin{bmatrix} t_{2,m} \\ t_{4,m} \\ t_{6,m} \\ t_{2n,m} \\ t_{2n-2,m} \\ t_{2n+2,m} \\ t_{2n-4,m} \\ l_{0,m} \\ l_{2,m} \\ l_{4,m} \\ l_{6,m} \\ l_{2n-2,m} \\ l_{2n,m} \\ r_{2(n-1),m} \end{bmatrix}, \quad
\boldsymbol{f}_1(\tilde{P}) = \begin{bmatrix}
\kappa\dfrac{\tilde{P}[3\rho(160\rho+69)+5]-5(96\rho+35)}{192(\tilde{P}+5\omega)} \\
\kappa\dfrac{60\rho+7-\tilde{P}[3\rho(20\rho+9)+1]}{48(\tilde{P}+5\omega)} \\
\dfrac{\kappa(\tilde{P}-3\omega)}{192(\tilde{P}+5\omega)} \\
0 \\ 0 \\ 0 \\ 0 \\
\tilde{P}\left[\dfrac{19\tilde{P}}{15(5\rho-1)\tilde{P}-75}+2\rho+\dfrac{49}{40}\right]-2 \\
\tilde{P}\left[\dfrac{58\tilde{P}}{15(5\rho-1)\tilde{P}-75}+6\rho+\dfrac{37}{10}\right]-6 \\
\dfrac{5\tilde{P}(\tilde{P}-3\omega)}{24(\tilde{P}+5\omega)} \\
0 \\ 0 \\ 0 \\ 0
\end{bmatrix},
$$

Please cite this article as: F.O. Falope, L. Lanzoni and E. Radi, Buckling of a Timoshenko beam bonded to an elastic half-plane: Effects of sharp and smooth beam edges, International Journal of Solids and Structures, https://doi.org/10.1016/j.ijsolstr.2019.08.034

$$
\boldsymbol{f}_{2n-1}(\tilde{P}) = \begin{bmatrix}
\kappa\left\{\tilde{P}\dfrac{n(n-1)\{5\rho[4n(n-1)(16\rho+5)-48\rho-47]-9\}+60\rho-12}{64n\{n[4n(n-2)+1]+3\}(\tilde{P}+5\omega)}+\ldots\right. \\
\left.\ldots+\dfrac{5[4+n(1-n)(16\rho+5)]}{64n(n-1)(\tilde{P}+5\omega)}\right\} \\
\dfrac{\kappa(40\rho+3)\left(\tilde{P}+(2n-3)(2n+1)\omega\right)}{32(2n-3)(2n+1)(\tilde{P}+5\omega)} \\
-\dfrac{\kappa\left(\tilde{P}+(2n-3)(2n+1)\omega\right)}{64(2n-3)(2n+1)(\tilde{P}+5\omega)} \\
\dfrac{\kappa}{32}\left[\dfrac{3}{n(1-2n)+1}-8\rho\right] \\
\dfrac{\kappa}{32}\left[8\rho+\dfrac{3}{n(2n-3)}\right] \\
\dfrac{\kappa}{32n(2n+1)} \\
-\dfrac{\kappa}{32[n(2n-5)+3]} \\
\left\{\tilde{P}^3\dfrac{5n\{n[4n(n-2)(24\rho-1)\omega+48\rho-17]+144\rho+13\}-6\omega}{8n[4n^2(n-2)+n+3](\tilde{P}+5\omega)}+\ldots\right. \\
\ldots+\tilde{P}^2\dfrac{n[120(n+3)\rho^2+(65-85n)\rho-3(n+1)]+6}{8n[4(2-n)n^2-n-3](\tilde{P}+5\omega)}+\ldots \\
\left.\ldots+\dfrac{15n[4n^2(n-2)\omega+n+3]}{n[4(2-n)n^2-n-3](\tilde{P}+5\omega)}\right\} \\
\dfrac{5[(2n-3)(2n+1)\omega+\tilde{P}](\tilde{P}-24\omega)}{4(2n-3)(2n+1)(5\omega+\tilde{P})} \\
\dfrac{5\tilde{P}}{8}\dfrac{(2n-3)(2n+1)\omega+\tilde{P}}{(3-2n)(2n+1)(5\omega+\tilde{P})} \\
0 \\
\dfrac{\tilde{P}}{4(1-n)} \\
\dfrac{\tilde{P}}{4n} \\
(2n-1)\omega
\end{bmatrix},
$$

$$
\boldsymbol{t}_{m\ Odd} = \begin{bmatrix} t_{-1,m} \\ t_{1,m} \\ t_{3,m} \\ t_{5,m} \\ t_{2n+1,m} \\ t_{2n-1,m} \\ t_{2n+3,m} \\ t_{2n-3,m} \\ l_{1,m} \\ l_{3,m} \\ l_{2n+1,m} \\ l_{2n-1,m} \\ z_{2n-1,m} \\ z_{1,m} \end{bmatrix}, \quad
\boldsymbol{g}_0(\tilde{P}) = \begin{bmatrix}
\dfrac{\kappa}{64}\left(48\rho-\dfrac{64}{\tilde{P}}+3\right) \\
\dfrac{\kappa}{64}\left(96\rho-\dfrac{64}{\tilde{P}}+7\right) \\
-\dfrac{\kappa}{64}(48\rho+5) \\
\dfrac{\kappa}{64} \\
0 \\ 0 \\ 0 \\ 0 \\
-\dfrac{\tilde{P}}{2} \\
\dfrac{\tilde{P}}{2} \\
0 \\ 0 \\ 0 \\
6\omega
\end{bmatrix},
$$

Please cite this article as: F.O. Falope, L. Lanzoni and E. Radi, Buckling of a Timoshenko beam bonded to an elastic half-plane: Effects of sharp and smooth beam edges, International Journal of Solids and Structures, https://doi.org/10.1016/j.ijsolstr.2019.08.034

$$\boldsymbol{g}_{2n}(\tilde{P}) = \begin{bmatrix} \frac{\kappa}{\tilde{P}}\frac{(128-64n^2-7\tilde{P})n^2+64(n^2-1)^2\rho\tilde{P}-5\tilde{P}-64}{64[n^2(4n^2-5)+1]} \\ \frac{\kappa}{\tilde{P}}\frac{64(\rho\tilde{P}-1)n^4+[128-(176\rho+15)\tilde{P}]n^2+(112\rho+3)\tilde{P}-64}{64[n^2(4n^2-5)+1]} \\ \frac{3\kappa(16\rho+3)}{64\left(4n^2-1\right)} \\ \frac{\kappa}{64(1-4n^2)} \\ \frac{1}{32}\kappa\left[\frac{3}{1-n(2n+1)}-8\rho\right] \\ \frac{1}{32}\kappa\left[8\rho+\frac{3}{n(2n+1)-1}\right] \\ \frac{\kappa}{32[n(2n+3)+1]} \\ \frac{\kappa}{32[n(3-2n)-1]} \\ \frac{3\tilde{P}}{2(4n^2-1)} \\ \frac{\tilde{P}}{2(1-4n^2)} \\ \frac{\tilde{P}}{2(2n+1)} \\ \frac{\tilde{P}}{2(1-2n)} \\ 2n\omega \\ \frac{6\omega}{1-4n^2} \end{bmatrix},$$

571 where $t_{i,j}, l_{i,j}, r_{i,j}$ and $g_{i,j}$ follows from Eqs. (42)–(45).

572 For smooth edges:

$$\boldsymbol{t}_{m\ Even} = \begin{bmatrix} r_{1,m} \\ r_{3,m} \\ r_{5,m} \\ r_{2n-1,m} \\ r_{2n+1,m} \\ r_{2n-3,m} \\ g_{0,m} \\ g_{2,m} \\ g_{4,m} \\ g_{2n-2,m} \\ g_{2n,m} \\ g_{2n-4,m} \end{bmatrix}, \quad \boldsymbol{f}_1(\tilde{P}) = \begin{bmatrix} \frac{\kappa}{48}\left(24\rho-\frac{16\tilde{P}}{5\omega+\tilde{P}}+15\right) \\ \kappa\frac{3[5\rho(16\rho+7)+1]\tilde{P}-5(48\rho+5)}{96(5\omega+\tilde{P})} \\ \kappa\frac{3\omega-\tilde{P}}{96(5\omega+\tilde{P})} \\ 0 \\ 0 \\ 0 \\ \frac{2\tilde{P}^2}{3(5\omega+\tilde{P})}-\frac{1}{8}(8\rho+5)\tilde{P}+1 \\ \frac{3}{80}\tilde{P}\left(80\rho-\frac{56\tilde{P}}{5\omega+\tilde{P}}+51\right)-3 \\ \tilde{P}\frac{5(\tilde{P}-3\omega)}{48(5\omega+\tilde{P})} \\ 0 \\ 0 \\ 0 \end{bmatrix},$$

$$\boldsymbol{f}_{2n-1}(\tilde{P}) = \begin{bmatrix} \frac{\kappa}{8}\left[\frac{4(n-2)(n+1)\tilde{P}}{(3-2n)(2n+1)(5\omega+\tilde{P})} + \frac{1}{n(1-n)} + 1\right] \\ 5\kappa\,\frac{(16\rho+1)[4n\omega(n-1)-3\omega+\tilde{P}]}{32(3-2n)(2n+1)(5\omega+\tilde{P})} \\ \kappa\,\frac{4(n1+)n\omega-3\omega+\tilde{P}}{32(2n-3)(2n+1)\left(5\omega+\tilde{P}\right)} \\ \frac{\kappa}{16}\left[8\rho + \frac{1}{(n-1)n}\right] \\ -\frac{\kappa}{16n(2n+1)} \\ -\frac{\kappa}{4[4n(2n-5)+12]} \\ \frac{\tilde{P}}{4}\left[\frac{4(n-2)(n+1)\tilde{P}}{(2n-3)(2n+1)(5\omega+\tilde{P})} + \frac{1}{n-1} - \frac{1}{n} - 1\right] \\ \frac{15[4(n-1)n\omega-3\omega+\tilde{P}](\tilde{P}-16\omega)}{16(2n-3)(2n+1)\left(5\omega+\tilde{P}\right)} \\ \frac{5\tilde{P}[4(n-1)n\omega-3\omega+\tilde{P}]}{16(3-2n)(2n+1)(5\omega+\tilde{P})} \\ \frac{(1-2n)[\tilde{P}-8(n-1)n\omega]}{8(n-1)n} \\ \frac{\tilde{P}}{8n} \\ \frac{\tilde{P}}{8(n-1)} \end{bmatrix},$$

$$\boldsymbol{t}_{m\ Odd} = \begin{bmatrix} r_{2,m} \\ r_{4,m} \\ r_{2n-2,m} \\ r_{2n,m} \\ r_{2n+2,m} \\ g_{1,m} \\ g_{3,m} \\ g_{2n-1,m} \\ g_{2n-3,m} \\ g_{2n+1,m} \end{bmatrix}, \quad \boldsymbol{g}_0(\tilde{P}) = \begin{bmatrix} \frac{\kappa}{8}(12\rho+1) \\ -\frac{\kappa}{32} \\ 0 \\ 0 \\ 0 \\ 6\omega - \frac{\tilde{P}}{2} \\ \frac{\tilde{P}}{4} \\ 0 \\ 0 \\ 0 \end{bmatrix}, \quad \boldsymbol{g}_{2n}(\tilde{P}) = \begin{bmatrix} \frac{\kappa}{4}\,\frac{6\rho+1}{1-4n^2} \\ \frac{\kappa}{32(4n^2-1)} \\ -\frac{\kappa}{16[n(2n-3)+1]} \\ \kappa\,\frac{2(4n^2-1)\rho+1}{4(4n^2-1)} \\ -\frac{\kappa}{16[n(2n+3)+1]} \\ \frac{\tilde{P}-6\omega}{4n^2-1} \\ \frac{\tilde{P}}{4(1-4n^2)} \\ \frac{n(8\omega n^2-\tilde{P}-2\omega)}{4n^2-1} \\ \frac{\tilde{P}}{4(2n-1)} \\ \frac{\tilde{P}}{4(2n+1)} \end{bmatrix},$$

where terms $g_{m,n}$ are defined according to Eq. (45).

Once matrix $\boldsymbol{A}(\tilde{P})$ has been assembled using relations (40) and (41), its determinant provides the system characteristic equation, i.e. the buckling spectrum whose roots are the dimensionless buckling loads $\tilde{P}_i$.

A3. Integral terms for the problem solution

The integral terms involved in the problem solution are:

$$t_{n,m} = \int_{-1}^{+1} \frac{T_n(\xi)T_m(\xi)}{\sqrt{1-\xi^2}}d\xi = \begin{cases} \pi/2, & \text{if } n = m \neq 0, \\ \pi, & \text{if } n = m = 0, \\ 0, & \text{if } n \neq m \end{cases} \tag{42}$$

$$l_{n,m} = \int_{-1}^{+1} T_n(x)T_m(x)\,dx = \begin{cases} \frac{\left(1-m^2-n^2\right)[(-1)^{m+n}+1]}{n^4-2\left(m^2+1\right)n^2+\left(m^2-1\right)^2}, & \text{if } n+m \text{ even} \\ 0, & \text{otherwise.} \end{cases} \tag{43}$$

$$r_{n,m} = \int_{-1}^{+1} U_{n-1}(x)T_m(x)\,dx = \begin{cases} \frac{2n}{n^2-m^2}, & \text{if } n+m \text{ odd} \\ 0, & \text{if } n+m \text{ even} \end{cases}, \tag{44}$$

$$g_{n,m} = \int_{-1}^{+1} \frac{U_n(x)T_m(x)}{\sqrt{1-x^2}}\,dx = \begin{cases} 0, & \text{if } n+m \text{ odd or } m > n \\ \pi, & \text{otherwise.} \end{cases} \tag{45}$$

Please cite this article as: F.O. Falope, L. Lanzoni and E. Radi, Buckling of a Timoshenko beam bonded to an elastic half-plane: Effects of sharp and smooth beam edges, International Journal of Solids and Structures, https://doi.org/10.1016/j.ijsolstr.2019.08.034

References

Baraldi, D., Tullini, N., 2018. In-plane bending of Timoshenko beams in bilateral frictionless contact with an elastic half-space using a coupled FE-BIE method. Eng. Anal. Bound. Elem. 97, 114–130.

Bazant, Z.P., Cedolin, L., 2003. Stability of Structures. Elastic, Inelastic, Fracture, and Damage Theories. Dover Publications, Inc..

Biot, M.A., 1937. Bending of an infinite beam on an elastic foundation. J. Appl. Mech. 4, 1–7.

Biot, M.A., 1957. Folding instability of a layered viscoelastic medium under compression. Proc. R. Soc. Lond. A 242 (1231), 444–454.

Falope, F.O., Lanzoni, L., Radi, E., Tarantino, A.M., 2016. Thin film bonded to elastic orthotropic substrate under thermal loading. J. Strain Anal. Eng.Des. 51 (4), 256–269.

Falope, F.O., Lanzoni, L., Tarantino, A.M., 2018. Modified hinged beam test on steel fabric reinforced cementitious matrix (SFRCM). Composites Part B 146, 232–243.

Foraboschi, P., 2009. Buckling of a laminated glass column under test. Struct. Eng. 87 (1), 2–8.

Gallagher, A.P., 1974. Buckling of a beam under axial compression with elastic support. Stud. Numer. Anal. 137–150.

Hetényi, M., 1971. Beams on Elastic Foundation: Theory with Applications in the Fields of Civil and Mechanical Engineering. University of Michigan.

Kachanov, M.L., Shafiro, B., Tsukrov, I., 2013. Handbook of Elasticity Solutions. Springer Science & Business Media.

Lanzoni, L., Radi, E., 2016. A loaded Timoshenko beam bonded to an elastic half plane. Int. J. Solids Struct. 92, 76–90.

Mace, B.R., Manconi, E., 2012. Wave motion and dispersion phenomena: veering, locking and strong coupling effects. J. Acoust. Soc. Am. 131 (2), 1015–1028.

Mason, J.C., Handscomb, D.C., 2002. Chebyshev Polynomials. Chapman and Hall/CRC.

Muskhelishvili, N.I., 2013. Some Basic Problems of the Mathematical Theory of Elasticity. Springer Science & Business Media.

Reynolds, O., 1886. IV. On the theory of lubrication and its application to Mr. Beauchamp tower's experiments, including an experimental determination of the viscosity of olive oil. Philos. Trans. R. Soc.London 177, 157–234.

Ruta, G.C., Elishakoff, I., 2006. Buckling of a column on a Wieghardt foundation. ZAMM 86 (8), 617–627.

Shield, T.W., Kim, K.S., 1992. Beam theory models for thin film segments cohesively bonded to an elastic half space. Int. J. Solids Struct. 29, 1085–1103.

Smith, T.E., 1969. Buckling of a beam on a Wieghardt-type elastic foundation. ZAMM 49 (11), 641–645.

Tezzon, E., Tullini, N., Lanzoni, L., 2016. A coupled FE-BIE model for the static analysis of Timoshenko beams bonded to an orthotropic elastic half-plane. Eng. Anal. Bound. Elem. 71, 112â;;128.

Timoshenko, S.P., Gere, J.M., 1961. Theory of Elastic Stability. McGraw-Hill, New York.

Tullini, N., Tralli, A., Baraldi, D., 2012. Buckling of Timoshenko beams in frictionless contact with an elastic half-plane. J. Eng. Mech. 139 (7), 824–831.

Tullini, N., Tralli, A., Baraldi, D., 2013. Stability of slender beams and frames resting on 2D elastic half-space. Arch. Appl. Mech. 83 (3), 467–482.

Wieghardt, K., 1922. Über den balken auf nachgiebiger unterlage. ZAMM 2 (3), 165–184.

Please cite this article as: F.O. Falope, L. Lanzoni and E. Radi, Buckling of a Timoshenko beam bonded to an elastic half-plane: Effects of sharp and smooth beam edges, International Journal of Solids and Structures, https://doi.org/10.1016/j.ijsolstr.2019.08.034